Accepted Manuscript

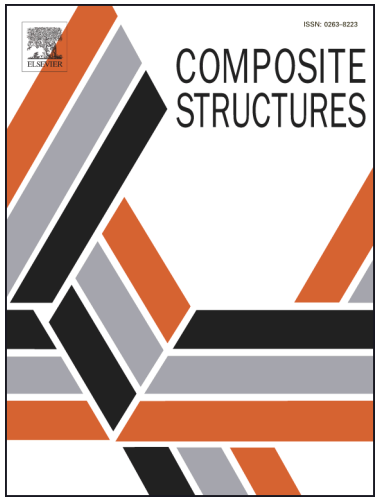

Seismic Performance of CFRP-Retrofitted Large-Scale Rectangular RC Columns under Lateral Loading in Different Directions

Daiyu Wang, Zhenyu Wang, Tao Yu, Hui Li

PII: S0263-8223(17)31283-7
DOI: https://doi.org/10.1016/j.compstruct.2018.03.029
Reference: COST 9476

To appear in: *Composite Structures*

Received Date: 22 April 2017
Revised Date: 19 January 2018
Accepted Date: 12 March 2018

Please cite this article as: Wang, D., Wang, Z., Yu, T., Li, H., Seismic Performance of CFRP-Retrofitted Large-Scale Rectangular RC Columns under Lateral Loading in Different Directions, *Composite Structures* (2018), doi: https://doi.org/10.1016/j.compstruct.2018.03.029

This is a PDF file of an unedited manuscript that has been accepted for publication. As a service to our customers we are providing this early version of the manuscript. The manuscript will undergo copyediting, typesetting, and review of the resulting proof before it is published in its final form. Please note that during the production process errors may be discovered which could affect the content, and all legal disclaimers that apply to the journal pertain.

Seismic Performance of CFRP-Retrofitted Large-Scale Rectangular RC Columns under Lateral Loading in Different Directions

Daiyu Wang[1,2,3]; Zhenyu Wang[1,2,3*]; Tao Yu[4]; Hui Li[1,2,3]

1. Key Lab of Structures Dynamic Behavior and Control of the Ministry of Education, Harbin Institute of Technology, Harbin, 150090, China.

2. Kay Lab of Smart Prevention and Mitigation of Civil Engineering Disasters of the Ministry of Industry and Information Technology, Institute of Technology, Harbin, 150090, China.

3. School of Civil Engineering, Harbin Institute of Technology, Harbin, 150090, China.

4. Faculty of Engineering and Information Sciences, University of Wollongong, Wollongong, NSW, 2522, Australia.

* Corresponding Author. Tel.: +86 451 8628 3856; Fax: +86 451 8628 3856.

E-mail address: zhenyuwang@hit.edu.cn (Z.Y. Wang)

Abstract: Considerable studies have been carried out on the seismic performance of fiber-reinforced polymer (FRP) retrofitted reinforced concrete (RC) columns. However, research on the seismic performance of FRP-retrofitted RC columns under lateral loading in different directions remains limited. This paper presents an experimental investigation on both un-retrofitted and carbon FRP (CFRP) retrofitted rectangular RC columns with an emphasis on the effect of the directions of lateral loading on the seismic performance of the columns. A total of ten large-scale cantilever rectangular RC columns were constructed and five of them were retrofitted with CFRP wraps at the potential plastic hinge regions. The overall performance of each specimen is examined in terms of damage evolution, lateral load-displacement hysteretic behavior, lateral strength, ductility capacity, stiffness degradation, and energy dissipation. The direction of lateral loading is found to have significant influence on the seismic performance of both un-retrofitted and CFRP-retrofitted rectangular RC columns. It is also found that the shear strength of the un-retrofitted and FRP-retrofitted rectangular RC columns in nonprincipal directions can be predicted based on the lateral strength in the principal directions by the ellipse equation.

Keywords: FRP; Rectangular RC columns; Seismic retrofit; Seismic performance; Lateral loading directions.

1. Introduction

As the main vertical members, columns are critical elements for the seismic performance of buildings. In the majority of earthquake cases, the collapse of reinforced concrete (RC) frame buildings is mainly caused by the failure of columns [1]. Therefore, numerous studies have been conducted on the seismic performance of RC columns [2-7]. It has been found that the most common causes of failure or severe damage of the RC columns are the lack of transverse confinement and ductility, inadequate shear or flexural capacity, and the strong-beam weak-column mechanism. In the past two decades, the use of externally bonded fiber-reinforced polymer (FRP) composites in the hoop direction has been found to be an effective strengthening/retrofitting method for improving the seismic performance of RC columns. As a result, considerable investigations on the seismic performance of RC columns strengthened/retrofitted with FRP have been conducted [8-17]. The majority of existing studies on the seismic performance of both RC columns and FRP-strengthened/retrofitted RC columns have been concentrated on the lateral loading in the principal direction of the columns. However, actual structures generally are subjected to multiaxial earthquake excitation. The seismic excitation loading can be in any direction. Moreover, the skewness also is another cause of maximum seismic response of FRP-retrofitted columns not being in the principal direction [18-19]. Consequently, it is essential to evaluate the effect of multi-directional lateral loading on the seismic performance of RC columns to develop more reliable design and strengthening/retrofitting procedures.

Thus far, the studies on the seismic performance of both RC columns and strengthened /retrofitted RC columns under multi-directional lateral loading are very limited, especially for FRP-strengthened/retrofitted RC columns. The limited available studies on RC columns have demonstrated that the failure mechanism of RC columns was significantly dependent on the loading path/direction. The ductility and energy dissipation capacity of the columns were also strongly affected by the loading path/direction. In addition, the biaxial cyclic lateral load was found to increase the strength and stiffness degradation when compared to the uniaxial load. Moreover, some

ACCEPTED MANUSCRIPT

ACCEPTED MANUSCRIPT

experimental evidenced that the plastic hinge-zone length tends to be stable around theoretical values and are not strongly affected by biaxial loading [20-26]. To the best of the authors' knowledge, only two experimental studies on the seismic performance of FRP-strengthened or retrofitted rectangular RC columns under biaxial loading have been conducted [27-28]. Dong et al. [27] conducted an experimental study on the seismic performance of CFRP-confined RC rectangular hollow bridge piers under unidirectional and bidirectional reverse lateral loads. The test results indicated that the damage of the columns was more serious and the failure process was accelerated when subjected to bidirectional earthquake action. The lateral load bearing capacity, ductility, stiffness and energy dissipation capacity were also reduced under bidirectional loading when compared with unidirectional loading. Rodrigues et al. [28] carried out an experimental campaign of RC columns and retrofitted RC columns subjected to biaxial cyclic loading actions. The experimental results show that the biaxial loading patterns have significant effects on the non-linear behavior and capacity of the columns. Due to the lack of investigations on the multi-directional seismic performance of FRP-retrofitted RC columns, there is no well-established design method to calculate the strength and ductility capacity of retrofitted RC columns.

To better understand the seismic performance and enrich the available experimental data of FRP-retrofitted RC columns under multi-directional loadings, this paper presents an experimental study in which 10 large-scale rectangular RC columns were tested under combined constant axial compression and reversed cyclic lateral displacements in different directions. Five columns were retrofitted with externally bonded carbon fiber-reinforced polymer (CFRP) wraps in the potential plastic hinge regions. The effect of lateral loading direction variation is evaluated in terms of damage evolution, lateral load-displacement hysteretic behavior, lateral strength, ductility capacity, stiffness degradation, and energy dissipation. The tests results of un-retrofitted and retrofitted columns are also compared to evaluate the efficiency of the CFRP retrofitted strategy.

2. Experimental program

2.1 Test specimens and material properties

ACCEPTED MANUSCRIPT

A total of 10 large-scale rectangular RC cantilever specimens representing half of building columns were prepared and tested under combined constant axial compression load and lateral reverse loading in different directions. The specimens were designed according to the out-of-date seismic design code of China (GBJ11-89) [29] to represent the numerous existing substandard RC frame columns. The specimens can be divided into two groups: five columns were tested without retrofitting as control specimens, and the other five corresponding columns were retrofitted by laterally wrapping three layers of unidirectional CFRP wraps in the potential plastic hinge zone. Each specimen has the identical rectangular cross section of 300 mm × 450 mm and a clear cantilever height (the part between the stub footing and the RC cuboid) of 1200 mm. To simulate a fixed-end boundary condition and single bending of the column, the columns were constructed with a strong concrete stub footing of dimensions 1500 mm × 650 mm × 600 mm. In addition, an RC cuboid with a dimension of 700 mm × 650 mm × 400 mm was also cast integrally at the top of each column in order to accommodate the connection of the lateral loading actuator.

All specimens had the same longitudinal and transverse reinforcement. Eight 20 mm diameter hot-rolled deformed steel bars were adopted as the longitudinal reinforcement, leading to a longitudinal reinforcement ratio of 1.86%. The longitudinal steel bars were anchored into the footing with a sufficient anchorage length. The transverse reinforcement of each column consisted of 8 mm diameter plain steel bars with a 135-degree hook. According to the out-of-date seismic design code (GBJ11-89) [29], the potential plastic hinge zone of columns should be provided with dense transverse reinforcement. For the first storey of RC frames, the height of densely spaced area of transverse reinforcement was 500 mm at the potential plastic hinge region of columns. As a result, the spacing of transverse reinforcement within and outside the potential plastic hinge region (i.e. 500 mm) in the present study was 100 mm and 200 mm, respectively, resulting in volumetric

transverse reinforcement ratios of 0.6% and 0.3%, respectively. Tensile tests on three bars were conducted for each type of reinforcing bars according to ASTM E8/E8M [30]. The measured average yield stresses were 430.7 MPa and 315.0 MPa for the longitudinal and transverse bars, respectively. The concrete cover thickness, measured to the outer side of the transverse reinforcing bars, was 30 mm for each column. The main variable in this study was the lateral loading direction, which varied from 0° (i.e. strong axis direction), 30°, 60°, 75° to 90° (i.e. weak axis direction). To simulate the variation of lateral loading direction, the clear cantilever part of the column (the part between the top of the stub footing and the bottom of the RC cuboid) was rotated about the vertical axis when constructed, as shown in Fig. 1(b) and Fig. 2(b). The dimensions and reinforcement details of the specimens are illustrated in Fig. 1.

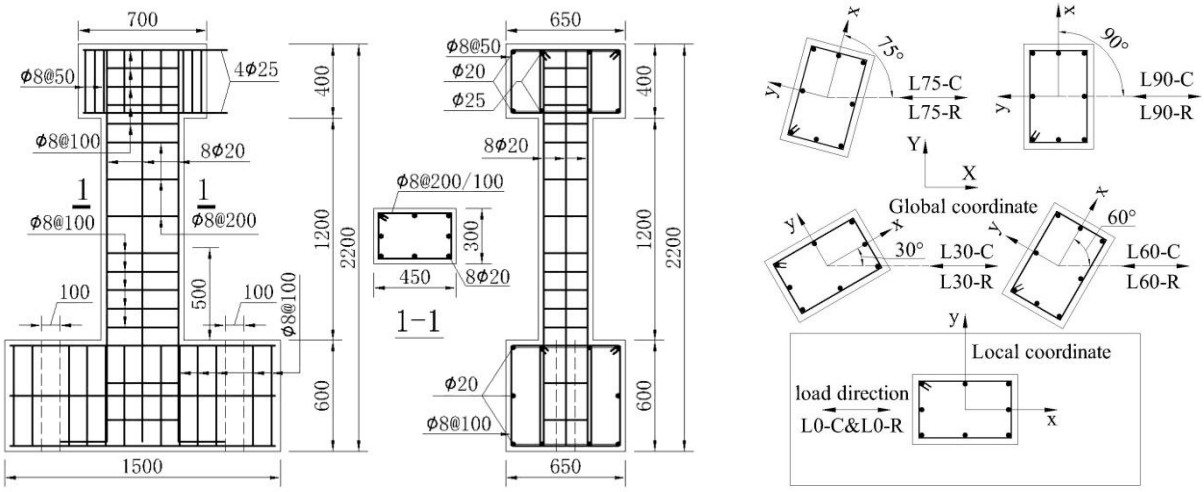

(a) Dimensions and reinforcement details for L0 series (b) Variation of lateral loading directions

Fig. 1 Specimen details (units: mm)

Table 1. Tested mechanical properties of steel reinforcement and CFRP

Material	Diameter/Thickness (mm)	Yield stress (MPa)	Tensile strength (MPa)	Elastic modulus (MPa)
Steel bars	8	315.0	382.7	194654
	20	430.7	656.5	214453
CFRP	0.167	-	4340	244000

One batch of commercial concrete was used to produce the specimens. The 28-day average

ACCEPTED MANUSCRIPT

compressive cylinder strength and that during the tests were 29.1 MPa and 38.2 MPa, respectively, according to axial compression tests on standard 150 mm × 300 mm cylinders. After 28 days standard curing, 5 specimens were retrofitted by wrapping 3 layers of unidirectional CFRP sheets laterally in the potential plastic hinge zone of the columns via a wet lay-up process. The epoxy resin consisted of two components (i.e. main agent and curing agent) was used to bond the CFRP wraps. The height of the wrapped region was 500 mm (i.e. approximately 1.11h, with h = height of the cross-section), which was the same as the densely spaced area of transverse reinforcement. The wrapped height was sufficient for the development of plastic hinge based on the existing studies on the plastic hinge length models [31-34]. For example, Sheikh and Khoury [31] suggested a plastic hinge length of 1.0h for columns under high axial loads. Tirasit and Kawashima's [32] tests showed that the length of damage zone was between 0.5D (with D = diameter of the circular cross section) and 1.5D for columns under different levels of loading. Other models [33-34] also provide similar predictions. Before applying CFRP, the concrete surface of the retrofitted region was slightly ground to form the desired corner radius. The corner radius for all the columns was equal to 0.1h (i.e. 45 mm). The CFRP wrap had a nominal thickness of 0.167 mm per layer, and the measured average tensile strength and elastic modulus from six flat coupon tests according to ASTM D3039 [35] were 4340 MPa and 241 GPa, respectively, based on the nominal thickness of CFRP. The tensile strength, compressive strength, bending strength, bonding strength with concrete surface, elastic modulus and elongation of epoxy resin after curing were 40.6 MPa, 75.4 MPa, 85.2 MPa, 4.1 MPa, 2800 MPa, and 1.7%, respectively. The details of mechanical properties of reinforcing bars and CFRP are summarized in Table 1. The specimen details are illustrated in Table 2. In the table, the name of the specimens starts with a letter "L" and a following number to represent lateral loading direction angle. The last letter "C" or "R" refers to the control or retrofitted columns. For example, specimen L30-R refers to a CFRP-retrofitted RC column tested under reverse lateral loading in an angle of 30° with respect to the strong axis of the column, as shown in Fig. 1(b).

ACCEPTED MANUSCRIPT

Table 2. Specimen details

Specimens		*b*×*h* (mm)	*H* (mm)	Longitudinal bars	Stirrups	*n*	CFRP layers	Load direction
Control	L0-C	300×450	1400	8ϕ20	ϕ8@100/200	0.40	0	0º
	L30-C							30º
	L60-C							60º
	L75-C							75º
	L90-C							90º
Retrofitted	L0-R						3	0º
	L30-R							30º
	L60-R							60º
	L75-R							75º
	L90-R							90º

Notes: *b*=width of cross section, *h*=height of cross section, *H*=height of column, *n*=axial compression ratio.

2.2 Test setup and instrumentation

The columns were subjected to a constant axial load and reverse lateral loads with different loading directions. In the present study, the constant axial load was equal to 2063 kN for all the specimens, leading to an axial compression ratio of 0.4 according to current Chinese design code of (GB50011-2010) [36].

$$n = P/Af_c \quad (1)$$

where P = applied axial load; f_c = cylinder compressive strength; and A = gross area of the column section.

At the beginning of the test, the axial load was slowly applied on the top of the specimens until the designed level was achieved and then maintained during the test. In order to enable the constant axial load to be maintained and moved with the upper part of the columns during test, a specific loading apparatus was utilized as shown in Fig. 2. In this case, the second-order effects (i.e. P-Δ effect) could be incorporated and simulated in the testing process.

The reverse lateral load was applied on the top of the columns by an electro-hydraulic actuator under displacement control mode. Considering the difference in the displacement capacity between the un-retrofitted and CFRP-retrofitted columns, two different lateral loading schemes were adopted, as shown in Fig. 3.

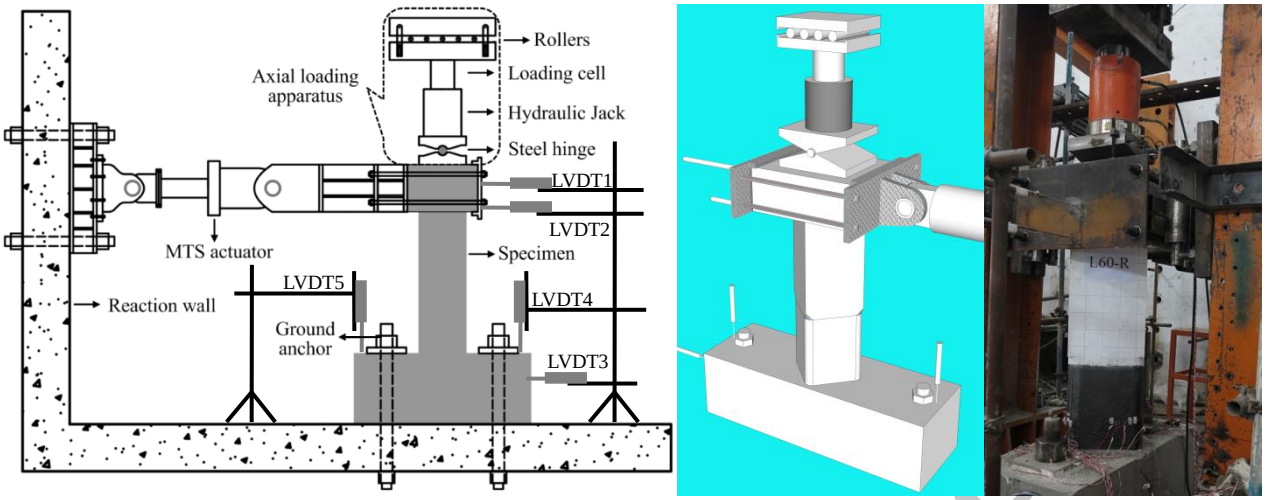

(a) Instrumentation details (b) schematic (c) photograph

Fig. 2 Test setup and instrumentation

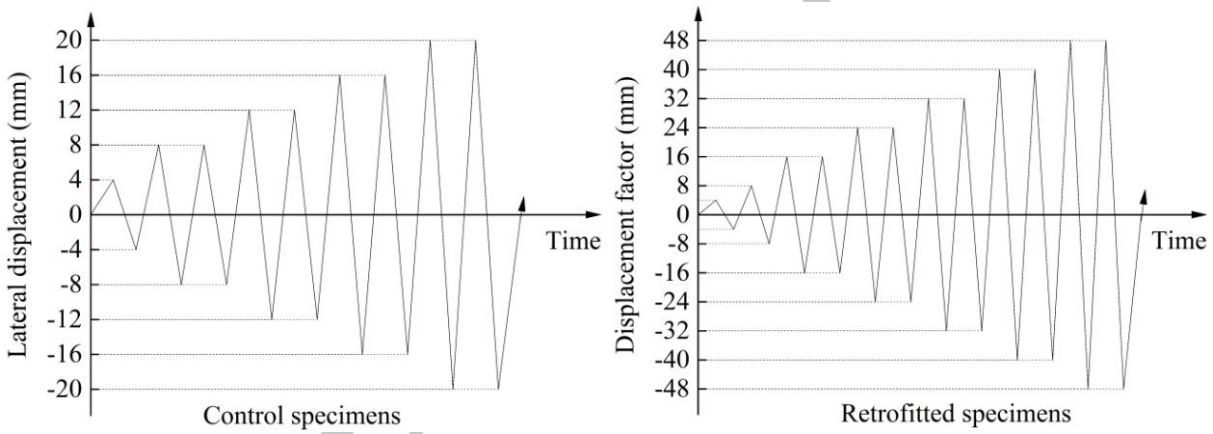

(a) Control specimens (b) Retrofitted specimens

Fig. 3 Lateral loading scheme

For the control specimens group, the displacement increment was set to be 4 mm and reversed twice at each level, except for the first displacement level which was repeated once only, as shown in Fig. 3(a). For all the specimens in the retrofitted specimens group, the first and second displacement levels were also increased with an increment of 4 mm and reversed once only, while the subsequent levels were increased with the imposed increment of 8 mm and reversed twice at each displacement level, as shown in Fig. 3(b). The tests were terminated when the columns lost over 30% of the lateral resistance capacity. The axial and lateral loads were measured by load cells. The lateral displacement was measured by three linear variable displacement transducers (LVDTs)

ACCEPTED MANUSCRIPT

along the height of columns (i.e. LVDT 1 to 3 in Figure 2a). Furthermore, two LVDTs (i.e. LVDT 4 and 5) were installed vertically to monitor the potential rotational displacement of the footing, as shown in Fig. 2(a).

3. Experimental results and discussions

3.1 General test observations and failure modes

The comparison of typical failure modes between the control and retrofitted specimens are shown in Fig. 4. It was found that the failure of the control specimens generally varied from brittle shear failure mode to ductile flexural failure mode with the variation of lateral load direction from the strong axis direction (i.e. 0°) to the weak axis direction (i.e. 90°). However, all the retrofitted specimens exhibited ductile failure mode despite the variation of lateral loading directions.

For the specimens tested in the strong axis direction (i.e. 0°), the control specimen L0-C finally exhibited a typical brittle shear failure mode. Initially, horizontal flexural cracks were formed on the tension side of the plastic hinge region at the lateral displacement level of 8 mm. Subsequently, the initial cracks widened and extended diagonally and more cracks occurred with the increase of lateral displacement. The concrete cover spalling was observed when the lateral displacement increased to 16 mm. No new cracks were formed after the lateral displacement reached 20 mm, but most existing diagonal cracks extended and widened. The concrete cover spalling area also increased with the increase of displacement level. Finally, a main diagonal shear crack extending the whole height of the column was formed at the displacement of 28 mm. The columns exhibited brittle failure mode due to the shear effect. The concrete in the plastic hinge region was also found to be severe spalled and crushed. The internal steel reinforcement in the column end was totally exposed. Outward bending of transverse reinforcement and buckling of longitudinal bars were evidently observed, as shown in Fig. 4(a). After retrofitted with CFRP at the potential plastic hinge region (i.e. L0-R), the brittle failure of the column was effectively prevented. One micro crack at the un-retrofitted regions was first observed at the same lateral displacement level of 8 mm. More cracks were formed and diagonally extended at the un-retrofitted region when the lateral

displacement reached 24 mm. The cracked area was between 0 mm to 400 mm above the CFRP wrapped region. However, no apparent damage was noticed at the retrofitted region except audible epoxy cracking at this stage. With the increase of lateral displacement, a few horizontal cracks on the CFRP wraps were formed. One main crack was formed at the height of 150 mm above the footing surface and the width increased up to about 2 mm when the displacement reached to 72 mm. Finally, the rupture of CFRP wraps occurred at this position, as shown in Fig. 4(b). In this case, however, the lateral resistance of the column was not rapidly reduced afterwards, and still remained about 70% of the tested peak load capacity. To further observe the damage of the retrofitted area, CFRP wraps were removed after the tests. It was observed that the concrete cover spalled, but the damage level was significantly reduced compared with the un-retrofitted control specimen L0-C. Buckling of longitudinal bars at the CFRP rupture position was also observed.

The failure process and final failure mode of the control (L30-C) and retrofitted column (L30-R) was similar as those of the corresponding specimens (i.e. L0-C and L0-R), respectively, despite the variation of lateral loading direction (i.e. from 0° to 30°). The control specimen L30-C also exhibited shear failure features. One main diagonal shear crack was formed at the end of the test, but the extending height was slightly smaller than that of the control specimen L0-C. The severe spalling and crushing of the concrete, outward bending of transverse reinforcement and buckling of longitudinal bars were also evidently observed at the plastic hinge region of the column, as shown in Fig. 4(c). For the retrofitted specimen L30-R, the final failure was changed to more ductile flexural mode similar to that of specimen L0-R. The horizontal and diagonal cracks on the concrete of the upper un-retrofitted regions and a few horizontal cracks on the CFRP wraps were also observed, but no rupture of CFRP wraps occurred at the end of test. After removal of wrapped FRP after test, it was found that the damage of the concrete was slightly less severe than that of the corresponding retrofitted specimen L0-R.

ACCEPTED MANUSCRIPT

(a) L0-C

(b) L0-R

(c) L30-C

(d) L30-R

(e) L60-C

(f) L60-R

(g) L75-C

(h) L75-R

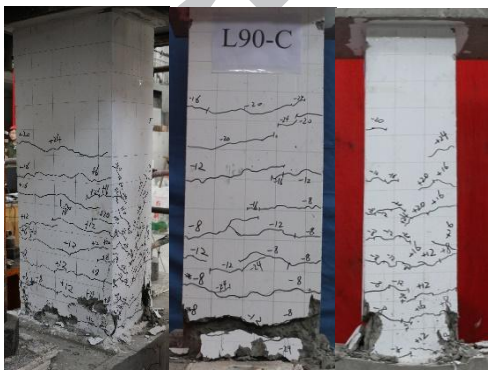

(i) L90-C

(j) L90-R

Fig. 4 Failure modes

With the lateral load direction increased to 60° and 75°, the damage processes of the control specimens (i.e. L60-C and L75-C) were similar to that of the corresponding control specimens

ACCEPTED MANUSCRIPT

tested with smaller angles of lateral loading (i.e. L0-C and L30-C), but the final failure changed to combined flexural-shear modes. The shear failure feature (i.e. diagonal cracks) became less evident and more flexural failure feature (i.e. horizontal cracks) was observed. The height of severe damaged area was also reduced and the damage was concentrated within the bottom 500 mm region, as shown in Fig 4 (e) and (g). After being retrofitted with CFRP (i.e. L60-R and L75-R), the deformation capacity of the columns was again significantly improved, but the lateral resistance was found to decrease more rapidly, compared with the retrofitted specimens tested with smaller angles of lateral loading (i.e. L0-R and L30-R). Removal of wrapped CFRP after test revealed that the concrete was only slightly crushed in the plastic hinge region, as shown in Fig 4 (f) and (h). This is due to the lateral stiffness was significantly reduced and shear span ratio increased with the increase of lateral loading angle increased. The lateral resistance of the columns will decrease with the decrease of lateral stiffness and increase of shear span ratio. However, the damage of concrete in the plastic hinge region has less influence on the lateral resistance of columns.

Both the control and retrofitted specimens exhibited flexural ductile failure mode when tested in the weak axis direction (i.e. L90-C and L90-R). For the un-retrofitted control specimen L90-C, the concrete was cracked very close to the horizontal direction and the severely damaged region was concentrated on the bottom end of the columns within a 200 mm height. Only a few of the internal steel reinforcing bars were exposed, as shown in Fig. 4(i). For the retrofitted specimen L90-R, the damage was effectively reduced compared to the corresponding control specimen L90-C. The CFRP wraps were found to be almost intact after test and the upper un-retrofitted region of the column was also not observed to exhibit significant damage except several horizontal cracks due to excessive flexural deformation. After removing the CFRP wraps, it was found that the concrete surfaces only suffered slight damage, as shown in Fig. 4(j).

3.2 Lateral load-displacement curves

The comparison of experimental lateral load-displacement hysteretic and envelop curves of each pair of control and retrofitted specimens subjected to lateral loading with the same direction is

shown in Fig. 5 and Fig. 6, respectively.

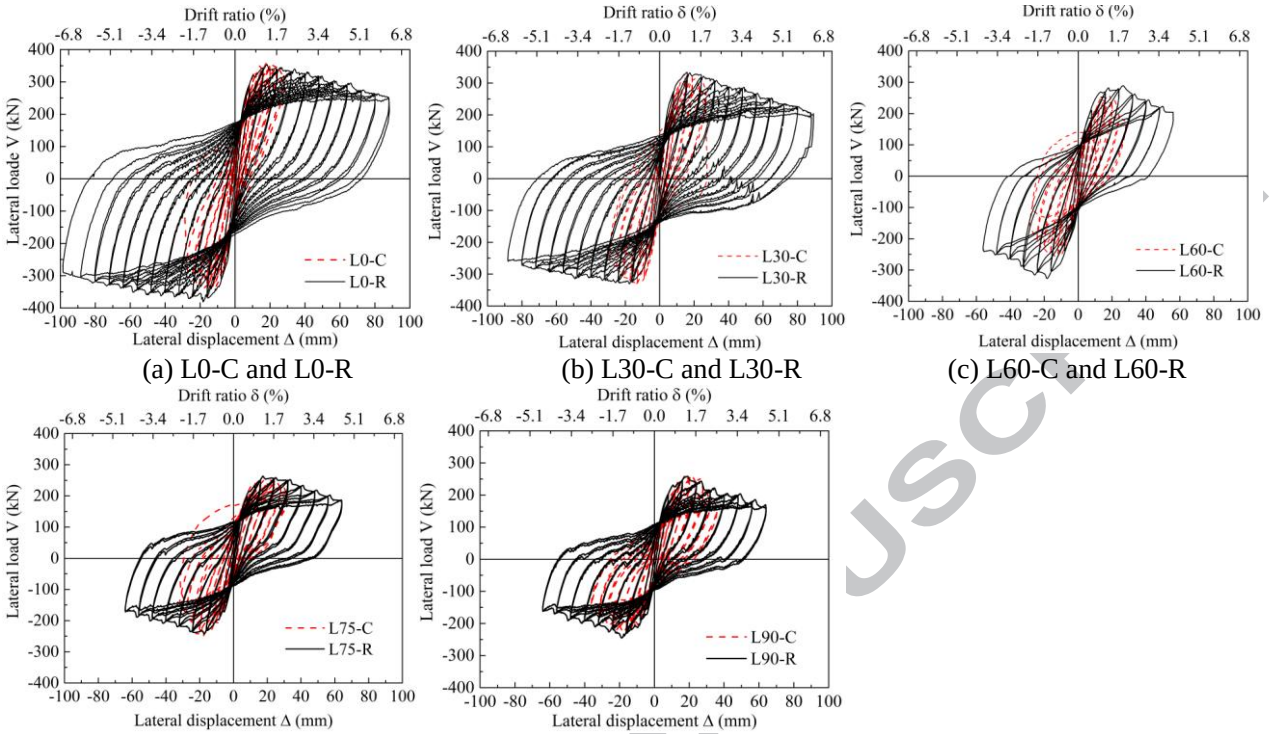

(a) L0-C and L0-R (b) L30-C and L30-R (c) L60-C and L60-R

(d) L75-C and L75-R (e) L90-C and L90-R

Fig. 5 Experimental lateral load-displacement hysteretic curves

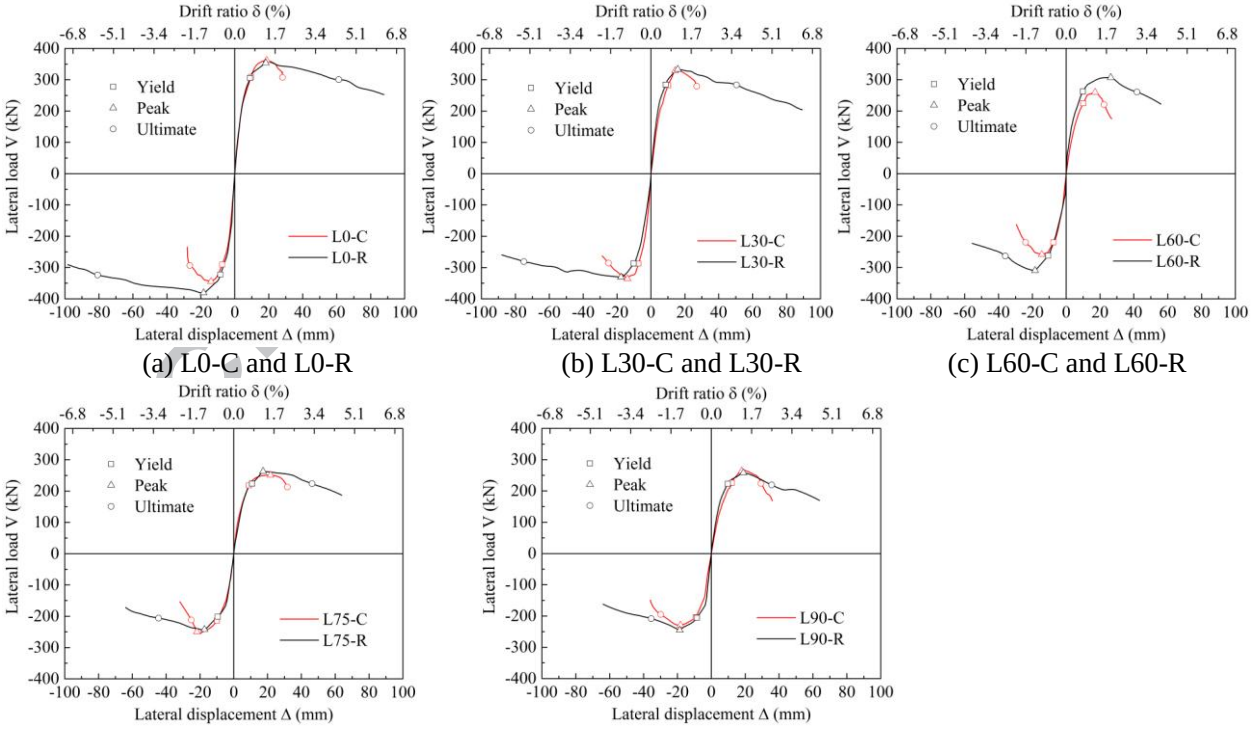

(a) L0-C and L0-R (b) L30-C and L30-R (c) L60-C and L60-R

(d) L75-C and L75-R (e) L90-C and L90-R

Fig. 6 Envelop curves for different loading directions

It is evident from Fig. 5 that the hysteretic behavior was significantly improved for each lateral loading direction after being retrofitted with CFRP, especially for the lateral loading in the 0° and

30° directions. The retrofitted columns exhibited much wider hysteretic loops and larger energy dissipation capacity than the corresponding control specimens for all loading directions. However, the enhancement in the hysteretic behavior decreased with the increase of loading direction angle (i.e. from 0° to 90°). It was also easily noted from Fig. 6 that the ductility of the columns was significantly increased after being retrofitted with CFRP, while the lateral load capacity was hardly increased except when loaded in the 60° direction. The ultimate lateral displacements were significantly enhanced due to the use of additional CFRP wraps, especially in the loading angles of 0° and 30°. The CFRP retrofitted columns also exhibited much more gradual post-peak strength degradation compared to the corresponding control specimens.

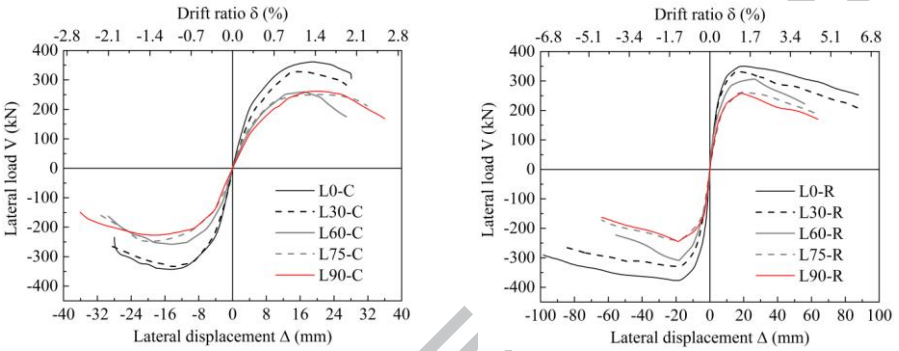

(a) Control specimens (b) Retrofitted specimens

Fig. 7 Comparison of envelop curves in all the loading directions

Fig. 7 shows the comparison of envelop curves in all the loading directions for control and retrofitted specimens, respectively. For control specimens, it is evident from Fig. 7(a) that the envelop curves has noticeable variations with the lateral loading angle changing from 0° to 60°. The peak lateral strength and initial stiffness were remarkably reduced when the angle of loading direction increased from 30° to 60°. After that, the variation of loading angle has slightly influenced on the envelop curves. The initial stiffness was slightly reduced, while the ductility was slightly enhanced with the increase of loading angle. Generally, it was found that the loading angle of 60° can be regarded as the weakest direction for rectangular RC columns. With this loading direction, the control column exhibited similar peak lateral strength and initial stiffness, but smaller peak and ultimate displacements and more rapid post-peak strength degradation than the corresponding column tested in the weak axis direction (i.e. 90°). For CFRP retrofitted specimens, the peak lateral

ACCEPTED MANUSCRIPT

strength and initial stiffness generally decreased with the increase of lateral loading angles, as shown in Fig. 7(b). Moreover, the rate of post-peak strength degradation (i.e. the slope of the descending branch) was approximately the same, except for the 60° direction. When loaded in this direction, the retrofitted specimens exhibited more rapid post-peak strength degradation and smaller ductility capacity. Similar to the control rectangular RC columns, it is demonstrated that the 60° angle of loading direction is another weak axis for CFRP retrofitted rectangular RC columns.

Table 3. Summary of test results

Specimen	Load direction		Δ_y (mm)	V_y (kN)	$K_y=\Delta_y/V_y$ (kN/mm)	Δ_c (mm)	V_c (kN)	Δ_u (mm)	δ_u (%)	$\mu=\Delta_u/\Delta_y$
L0-C	0°	+	9.56	308.42	32.26	18.79	361.77	28.08		
		-	7.40	290.17	39.21	13.97	344.86	26.50		
		AVG	**8.48**	**299.30**	**35.29**	**16.38**	**353.32**	**27.29**	**1.95**	**3.22**
L0-R		+	9.02	305.57	33.88	18.26	353.63	61.17		
		-	8.44	322.54	38.22	18.37	380.73	80.77		
		AVG	**8.73**	**314.06**	**35.97**	**18.32**	**367.18**	**70.97**	**5.07**	**8.13**
L30-C	30°	+	10.16	282.06	27.76	14.26	328.78	26.99		
		-	7.38	287.49	38.96	13.88	335.96	25.06		
		AVG	**8.77**	**284.78**	**32.47**	**14.07**	**332.37**	**26.03**	**1.86**	**2.97**
L30-R		+	8.69	284.45	32.73	15.78	333.61	50.44		
		-	10.12	286.98	28.36	17.69	330.62	74.99		
		AVG	**9.41**	**285.72**	**30.36**	**16.74**	**332.12**	**62.72**	**4.48**	**6.67**
L60-C	60°	+	10.09	224.75	22.27	17.08	260.00	22.35		
		-	7.48	219.64	29.36	14.41	258.33	24.02		
		AVG	**8.79**	**222.20**	**25.28**	**15.75**	**259.17**	**23.19**	**1.66**	**2.64**
L60-R		+	9.93	262.56	26.44	26.37	307.00	41.83		
		-	10.57	261.88	24.78	18.40	309.39	35.99		
		AVG	**10.25**	**262.22**	**25.58**	**22.39**	**308.20**	**38.91**	**2.78**	**3.80**
L75-C	75°	+	9.06	218.05	24.07	21.78	250.90	31.70		
		-	9.94	214.19	21.55	21.76	249.69	25.11		
		AVG	**9.50**	**216.12**	**22.75**	**21.77**	**250.30**	**28.41**	**2.03**	**2.99**
L75-R		+	10.78	223.46	20.73	17.34	263.07	46.33		
		-	9.52	201.65	21.18	17.34	242.43	44.47		
		AVG	**10.15**	**212.56**	**20.94**	**17.34**	**252.75**	**45.40**	**3.24**	**4.47**
L90-C	90°	+	12.18	226.09	18.56	17.90	263.80	29.28		
		-	9.18	204.17	22.24	18.20	229.17	29.90		
		AVG	**10.68**	**215.13**	**20.14**	**18.05**	**246.49**	**29.59**	**2.11**	**2.77**
L90-R		+	9.74	222.67	22.86	18.91	258.23	35.61		
		-	8.53	205.62	24.11	18.62	245.29	35.48		
		AVG	**9.14**	**214.15**	**23.43**	**18.77**	**251.76**	**35.55**	**2.54**	**3.89**

Notes: Δ_y and V_y = yield displacement and corresponding strength; $K_y=\Delta_y/V_y$ initial stiffness; Δ_c and V_c = peak displacement and corresponding strength; Δ_u and δ_u = ultimate displacement and drift ratio; $\mu=\Delta_u/\Delta_y$ ductility factor.

ACCEPTED MANUSCRIPT

3.3 Lateral strength

To investigate and evaluate quantitatively the variation in the seismic performance, the lateral displacement and the corresponding strength at the yield (i.e. Δ_y and V_y), peak (i.e. Δ_c and V_c), and ultimate (i.e. Δ_u and V_u) points were obtained from the envelop curves, as summarized in Table 3. The definition of yield point was determined by the widely accepted energy method which was proposed by Mahin and Bertero [37-38], as illustrated in Fig. 8. The ultimate point refers to the point where the lateral load was reduced to 85% of the peak load. It is evident from Table 3 that the yield and peak lateral strength of control and retrofitted specimens both generally decreased with the increase of loading angle.

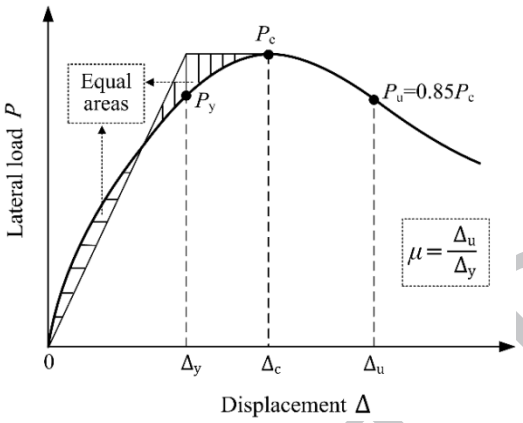

Fig. 8 Energy method

Fig. 9 shows the relationship between the lateral strength of all the specimens and the angle of lateral loading. In the figure, the two experimental lateral strengths in the weak and strong axes (i.e. V_x and V_y) are linked by the ellipse equation as follows:

$$\frac{V_{\alpha x}^2}{V_x^2}+\frac{V_{\alpha y}^2}{V_y^2}=1 \qquad (2)$$

where V_x and V_y are the lateral strength in the strong and weak axis directions (i.e. 0° and 90°); $V_{\alpha x}=V_\alpha\cdot\cos\alpha$ and $V_{\alpha y}=V_\alpha\cdot\sin\alpha$ are the components of lateral strength in the diagonal direction when projecting to the strong and weak axis directions; $V_\alpha=\sqrt{V_{\alpha x}^2+V_{\alpha y}^2}$ is the lateral strength in diagonal direction with angle of α degree. In other words, the shear strength of rectangular columns in nonprincipal directions can be predicted based on the shear strength in principal

ACCEPTED MANUSCRIPT

ACCEPTED MANUSCRIPT

directions.

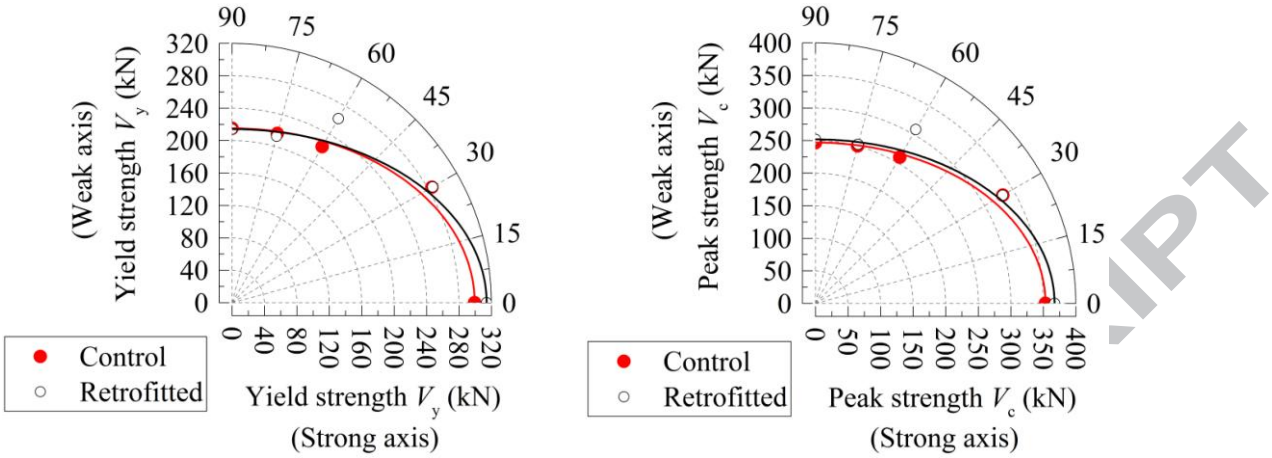

(a) Yield strength (b) Peak strength

Fig. 9 Lateral strength versus loading directions

It is evident from Fig. 9 (a) that both the yield strength and peak strength of control specimens followed approximately the ellipse line. The test values of the lateral strengths in the loading angles of 30°, 60° and 90° are all consistent with the predictions of the ellipse equation. For the FRP retrofitted specimens, both the yield and peak strength were also generally consistent with the ellipse curve, except for the 60° direction. In this direction, the test results are obviously larger than the predicted values of Eq.(2), as shown in Fig. 9(b). In addition, it is easily observed from Table 3 and Fig. 9 that both the yield and peak strengths of the rectangular RC columns were only slightly enhanced after being retrofitted with CFRP. Moreover, the enhancement also generally decreased with the increase of loading direction angles, except for the 60° direction. For example, the average increase in the peak strength after being retrofitted with CFRP was about 3.92% and 2.14% in the 0° and 90°, respectively, but the increase reached 18.92% in the 60° direction. Previous discussion in Fig. 7 has shown that the angle of 60° can be regarded as another weak axis. The larger increase indicated that the lateral load bearing capacity was effectively improved in this weak direction after being retrofitted with CFRP.

From the above discussions, it can be concluded that the lateral strength of un-retrofitted rectangular RC columns in nonprincipal directions can be reasonably predicted based on the lateral strengths in the principal directions using the ellipse equation, while the lateral strength of

ACCEPTED MANUSCRIPT

retrofitted columns can be conservatively predicted using the same equation. The current Chinese Code for Design of Concrete Structures (GB50010-2010) [39] also specified that the shear capacity of rectangular RC columns in nonprincipal directions followed the ellipse rule. Considering the earthquake action, the shear capacity of rectangular RC columns in the two principal directions (i.e. strong and weak axis directions) can be predicted by the following equations [39]:

$$V_{ux} = \frac{1}{\gamma_{RE}}\left(\frac{1.05}{\lambda_x + 1} f_t b h_0 + f_{yv}\frac{A_{svx}}{s} h_0 + 0.056N\right) \quad (3)$$

$$V_{uy} = \frac{1}{\gamma_{RE}}\left(\frac{1.05}{\lambda_y + 1} f_t h b_0 + f_{yv}\frac{A_{svx}}{s} b_0 + 0.056N\right) \quad (4)$$

where, V_{ux} and V_{uy} = shear capacity in the two principal directions (i.e. x and y directions); γ_{RE} = adjustment coefficient of seismic resistance, which is taken as 0.85 for shear capacity; b and h = width and depth of rectangular cross section; b_0 and h_0 = effective width and depth of rectangular cross section; $\lambda_x = H_n/2h_0$ and $\lambda_y = H_n/2b_0$ are the shear span ratio of RC frame columns in x and y direction, respectively; The shear span ratio (λ) was specified between 1 to 3, the value is equal to 1 if calculated actual value is smaller than 1 and equal to 3 if larger than 3; H_n = clear height of column; f_t = tensile strength of concrete; f_{yv} = yield strength of transverse steel reinforcement; A_{svx} and A_{svy} = total cross-sectional area of transverse reinforcement parallel to x and y direction, respectively; s = center to center spacing of transverse reinforcement; N = axial compression load, which is no larger than $0.3f_cA$. Then, the shear resistance of rectangular RC columns in any direction can be predicted based on the Eq. (2) to (4).

Fig. 10 presents the comparison between the test results and predictions of the shear resistance model. It should be noted that the strengthening scheme was designed for seismic retrofit of columns. The purpose was in order to gain more ductility. Therefore, the FRP wraps were applied laterally at the potential plastic hinge regions only. The previous discussions have also demonstrated that the wrapped FRP has little influence on the peak strength of columns, as shown in Fig. 9. Consequently, the critical section to calculate the shear capacity of FRP-retrofitted columns was the

ACCEPTED MANUSCRIPT

same as that of control specimens, which is the cross section of un-retrofitted region with the hoop spacing of 200 mm.

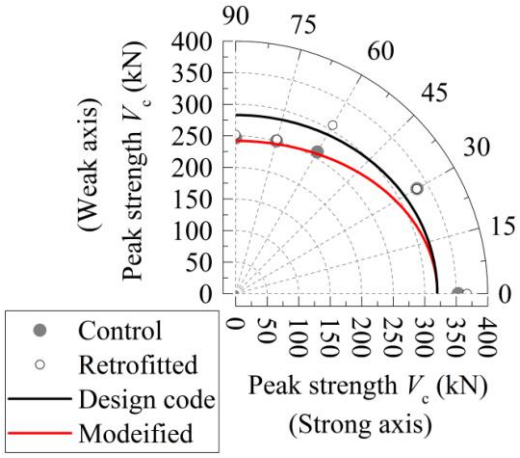

Fig. 10 Comparison between experimental and predicted peak strengths

It is evident from Fig. 10 that the predicted results were larger than the test values of control specimens and CFRP-retrofitted specimens when the lateral loading angle becomes larger than 30° and 60°, respectively. It means that the shear resistance of rectangular columns will be overestimated by the shear strength equitation of current design code in the angle of about 30° to 90° directions. This is mainly due to the fact that the design code specifies the maximum limit value of shear span ratio is equal to 3.0 when calculating the shear resistance of rectangular RC columns by Eq. (3) and (4). In this case, the predicted shear strength will be larger than that calculated using real shear span ratio for columns with a shear span ratio larger than 3.0. In the present study, the shear span ratio in the weak axis direction (i.e. 90°) was about 4.7. The predicted shear strength was approximately the same as the test results in the larger angle of loading directions if calculated using the real shear span ratio by the Eq. (2) to (4), as shown in Fig. 10. It is indicated that the maximum limit value of shear span ratio is specified equal to 3.0 may not be safe for designing of rectangular RC columns with a larger shear span ratio.

3.4 Displacement and ductility factor

The variation of lateral displacement and ductility factor versus angle of loading directions is plotted in Fig. 11.

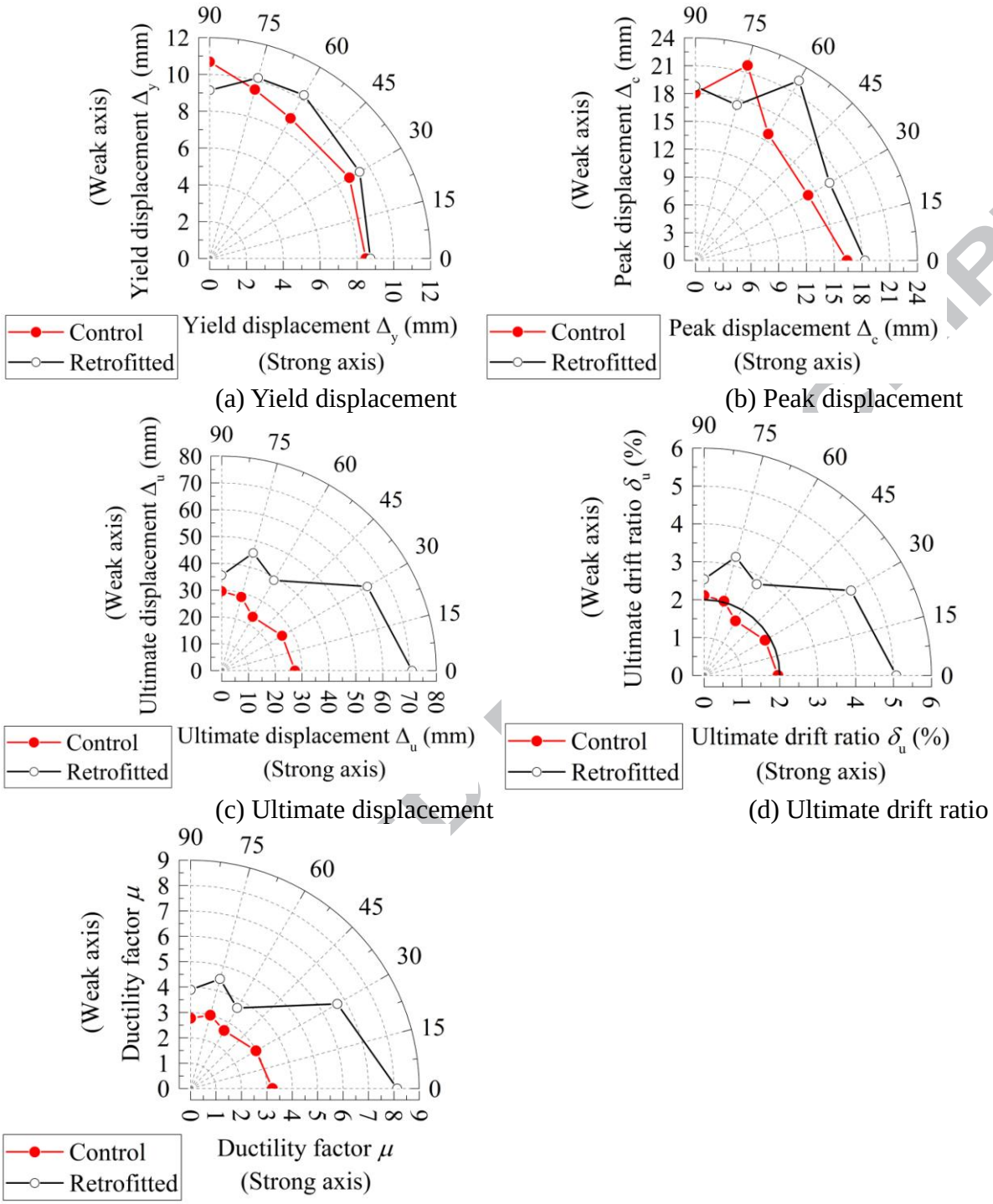

Fig. 11 Lateral displacement and ductility factor versus loading directions

It is evident form Table 3 and Fig. 11 (a) that the yield displacement (Δ_y) of control specimens slightly increased with the increase of angle of loading directions. There was an increase of approximately 3.42%, 3.66%, 12.03%, 25.94% when the angles changed from 0° to 30°, 60°, 75° and 90°, respectively. After being retrofitted with CFRP, the yield displacement of the columns also generally increased when the loading direction angles were not larger than 60°. After that, the yield

displacement started to decrease with the increase of loading direction angles, as shown in Fig. 11(a). For example, the yield displacement of the retrofitted columns was 8.73 mm, 10.25 mm and 9.14 mm for the directions of 0°, 60°, and 90°, respectively.

Table 3 and Fig. 11 (b) also show that both the control and retrofitted specimens exhibited similar variation trend of peak displacement (Δ_c) versus lateral loading direction angles. The peak displacement was slightly reduced when the lateral loading angle changed from 0° to 30°. After that, the peak displacement increased with the increase of loading angle. The peak displacement reached the maximum value at the angles of 60° and 75° for the retrofitted and control specimens, respectively. Then, the value was reduced again with the loading angle.

It is evident from Table 3 and Fig. 11 (c) and (d) that the ultimate displacement (Δ_u) and drift ratio (δ_u) were both significantly enhanced due to the use of additional CFRP wraps at the plastic hinge region. However, the enhancement was generally reduced with an increase of loading direction angles. The increment in Δ_u and δ_u after being retrofitted with CFRP was approximately 160.06%, 140.95%, 67.79%, 59.80%, 20.14% for the loading direction angels of 0°, 30°, 60°, 75°, and 90°, respectively. In addition, it can also be observed that the control specimens exhibited the minimum Δ_u for the 60° direction loading rather than loading in the weak axis direction (i.e. 90°). The ultimate drift ratios for the loading directions of 0° to 60° were all smaller than the requirement of the ultimate inter-story drift ratio (i.e. 2.0%) specified by the current Chinese Code for Seismic Design of Buildings (GB5011-2010) [36], while the values just satisfied the requirement for the loading directions of 75° and 90°, as shown in Fig. 11 (d). The minimum Δ_u of CFRP-retrofitted specimens appeared in the weak axis direction (i.e. 90°), but the column also exhibited less ultimate deformation capacity in the 60° direction. The Δ_u in the 90° direction was 35.55 mm, while the value in the 60° direction was only slightly larger (i.e. 38.91 mm). However, the δ_u of CFRP-retrofitted specimens was well above the 2% requirement despite of the loading directions. The δ_u in the strong axis direction (i.e. 0°) increased to 5.07%, which is more than twice the 2% requirement. Moreover, the δ_u in the weak directions of 60° and 90° were about 2.78% and 2.54%,

ACCEPTED MANUSCRIPT

respectively, which were still 39% and 27% larger than the requirement, respectively.

Ductility factor (μ) is defined as the ultimate displacement (Δ_u) divided by the yield displacement (Δ_y), which can directly reflect the plastic deformation capacity of structures and members. It can be easily observed from Fig. 11 (e) and Table 3 that the ductility factor of the retrofitted columns was also remarkably improved compared to the corresponding control columns in all the loading directions, especially in the 0° and 30° directions. Moreover, the control specimens exhibited similar plastic deformation capacity, but slightly worse in the 60° direction. The plastic deformation capacity of retrofitted columns generally decreased with the increase of loading direction angles, while the worst plastic deformation capacity also appeared in the 60° angle of loading direction. For example, after being retrofitted with CFRP, the μ improved from 3.22 to 8.13 and 2.77 to 3.89 in the direction of 0° and 90°, respectively, while the value increased from 2.64 to 3.80 in the 60° direction. There was an increment in the plastic deformation capacity of approximately 152.48%, 43.94%, 40.43% in the directions of 0°, 60° and 90°, respectively.

It is evident from the preceding comparisons and discussions that both control and CFRP retrofitted rectangular RC columns generally exhibited worst ultimate lateral deformation and plastic deformation capacities in the 60° direction, even much worse than in the weak axis direction (i.e. 90°). This is consistent with the previous observation that the loading angle of 60° was another weak axis or even the weakest axis of un-retrofitted and retrofitted rectangular RC columns.

3.5 Stiffness degradation

The initial stiffness and effective stiffness were crucial parameters in the displacement-based design method. The initial stiffness was usually determined based on the yield point of load-displacement envelop curve. In the present study, the initial stiffness (K_y) and effective stiffness (K_e) are defined as the secant stiffness at the theoretical yield point that is obtained by the energy method and the secant stiffness at unloading point of each displacement level, respectively. The initial stiffness of both control and retrofitted specimens is illustrated with respect to its loading direction angles in Fig. 12.

ACCEPTED MANUSCRIPT

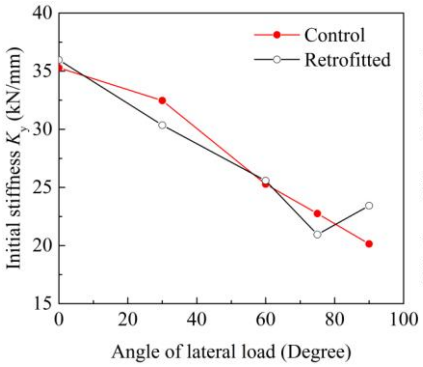

Fig. 12 Initial stiffness

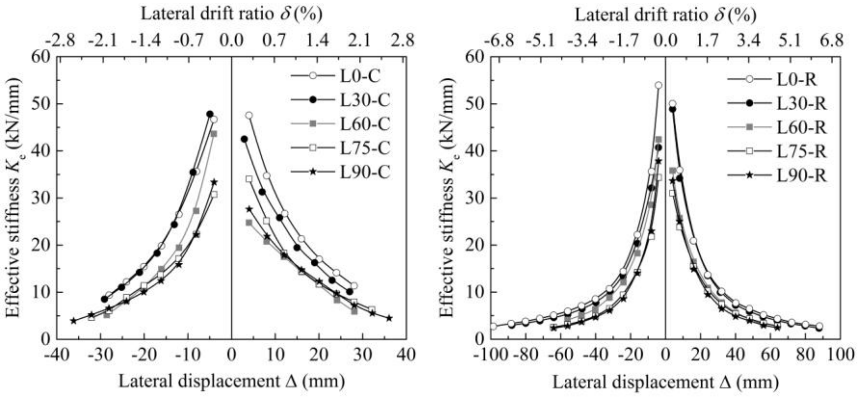

(a) Control specimens (b) Retrofitted specimens

Fig. 13 Comparison of effective stiffness

It is evident that the initial stiffness of control specimens was reduced with the increase of loading direction angles. The initial stiffness was reduced approximately 7.99% when loading changed from the strong axis direction (i.e. 0°) to the 30° direction. After that, the initial stiffness reduced approximately linearly. The initial stiffness was observed to decrease by 42.93% when the loading direction finally changed to the weak axis direction (90°). A similar trend was observed for CFRP retrofitted specimens. The initial stiffness of retrofitted specimens also remarkably decreased approximately in an approximately linear trend when the loading direction angle increased from 0° to 75°. However, the only difference is that the initial stiffness slightly increased when the loading direction changed from 75° to 90°. There was a decrease in the initial stiffness of about 41.78% when the angle of loading direction increased from 0° to 75°, while this value was about 34.86% when loading direction increased from 75° to 90°. It is also evident from Fig. 12 that the initial stiffness of control and retrofitted specimens only exhibited slightly difference for each direction, suggesting that the FRP strengthening had only a small effect on the initial stiffness of the columns. This is not difficult to understand as the columns were seismic retrofitted, and the CFRP wraps were applied laterally in the potential plastic hinge regions only.

The comparison of effective stiffness versus lateral displacement in all loading directions is shown in Fig. 13. It is evident that both the control and retrofitted specimens exhibited similar trend of effective stiffness degradation despite the angles of loading direction. The effective stiffness was reduced rapidly with an increase of lateral displacement in the initial stage, while the rate of

ACCEPTED MANUSCR

degradation become much more gradual when the lateral displacement level increased to about 15 mm to 20 mm, which is approximately equal to the displacement of peak point as shown in Table 3. However, the effective stiffness at the same displacement level generally decreased with the increase of loading direction angle, especially in the initial stage. For control specimens as shown in Fig. 13(a), the effective stiffness at each displacement level was obviously reduced in the positive direction (i.e. push) when the loading angle increased from 0° to 30°, while the values at each level were significantly reduced in both push and pull direction when the angle of loading direction further increased to 60°. After that, the remarkable decrease of the effective stiffness with the increase of loading angle was only observed in the initial stage. There was a decrease in the effective stiffness at the first displacement level (i.e. 4 mm) by about 40% to 50% when the loading direction changed from 0° to 90°. After the lateral displacement level reached about 15 mm to 20 mm, the effective stiffness at each displacement level was approximately the same for control specimens load in large angle of 60° to 90°, indicating that the variation of loading directions has very slight effect on the effective stiffness degradation at large lateral displacement and lateral loading angle. For retrofitted specimens, similar observations can also be found from Fig. 13(b). In the pull direction, the effective stiffness at each displacement level gradually decreased with the increase of loading direction angle until 75°. In the push direction, the effective stiffness was approximately the same at each similar displacement level when the loading direction changed from 0° to 30°, and from 60° to 90°. Remarkable decrease of effective stiffness at each level was only observed when the loading angle increased from 30° to 60°. The maximum decrease of effective stiffness at the displacement level (i.e. 4 mm) was about 35% to 40% when the loading direction varied from strong axis to weak axis.

The effective stiffness degradation of control and retrofitted specimens in each loading direction is illustrated in Fig. 14. It is evident that the effective stiffness degradation behavior of control and retrofitted specimens is approximately the same at the initial stage in most loading directions, except in the 60° direction. After the lateral displacement level reached about 20 mm,

ACCEPTED MANUSCRIPT

which is approximately the same as the peak displacement, the control specimens generally exhibited a more serious degradation in the effective stiffness than the retrofitted specimens. This is consistent with the previous observation that the control specimens exhibited much more rapid post-peak strength degradation than that of the retrofitted specimens, as shown in Fig. 6. A comparison between the control specimen L60-C and the retrofitted specimen L60-R shows that the degradation of effective stiffness in the other weak direction (i.e. 60°) was obviously reduced under the same displacement level, as shown in Fig. 14 (c). This is also consistent with the previous observation that the column exhibited the maximum enhancement in the lateral load bearing capacity, and the most pronounced reduction of post-peak strength degradation behavior in the 60° direction after being retrofitted with CFRP.

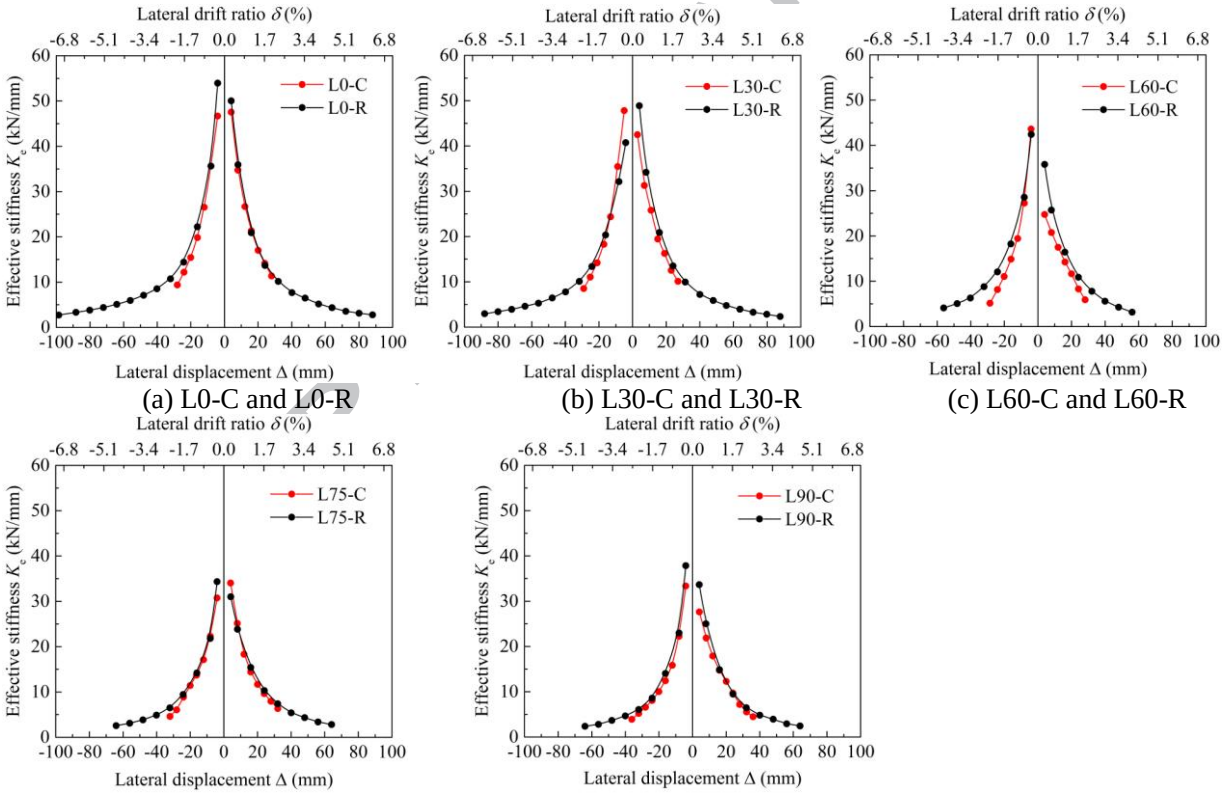

(a) L0-C and L0-R (b) L30-C and L30-R (c) L60-C and L60-R

(d) L75-C and L75-R (e) L90-C and L90-R

Fig. 14 Comparison of effective stiffness between control and retrofitted specimens

3.6 Energy dissipation

The energy dissipation capacity is one of the important indexes to evaluate the seismic performance of RC members and structures. The hysteretic dissipated energy is defined as the area enclosed by the lateral load-displacement hysteretic curves [40]. In the present study, the energy

NUSCRIPT

dissipation of the first hysteretic loop at each displacement level was computed. Fig. 15 shows the hysteretic energy dissipation of each single loop versus lateral drift ratio for all the specimens.

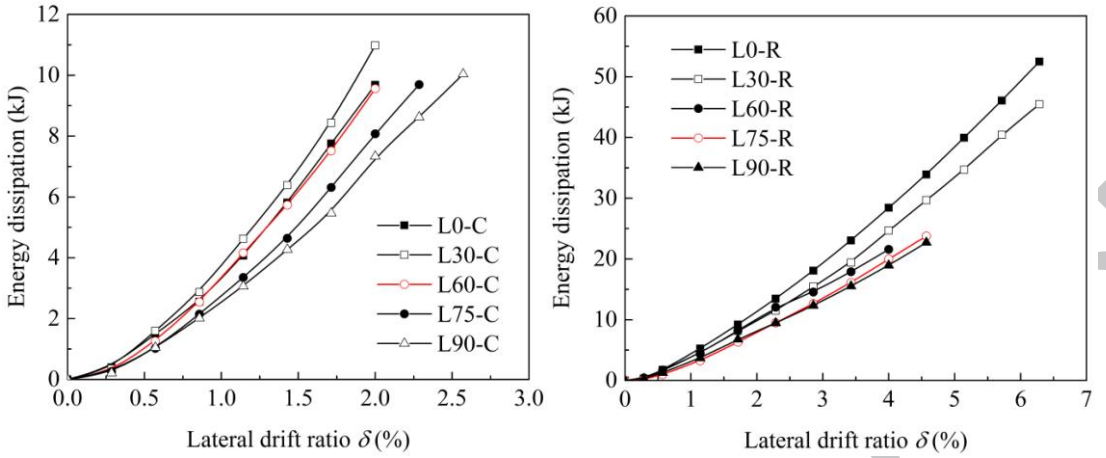

(a) Control specimens (b) Retrofitted specimens

Fig. 15 Energy dissipation of single hysteretic loop at each drift ratio level

It is obvious from Fig. 15 (a) that the energy dissipation capacity of control specimens was improved as the loading direction rotated from 0° to 30°. After that, the energy dissipation gradually decreased with the loading angle. Specimens L0-C and L60-C exhibited approximately the same hysteretic energy dissipation capacity at the same displacement levels. This result is different with the previous observation that the lateral strength of the columns gradually decreased with the increase of loading direction angle. The difference was due to the variation of hysteretic behavior with the increase of loading direction angle. Fig. 16 (a) shows the comparison of hysteretic loops of specimens L0-C, L30-C, and L60-C at the displacement level of 20 mm. It is evident that the lateral strength was only slightly reduced when the loading direction rotated from 0° to 30°, but the whole lateral load-displacement loop became much wider. Consequently, the total enclosed area within load-displacement loop of specimen L30-C was slightly larger than that of specimen L0-C. For specimen L60-C, the lateral strength was obviously reduced but the hysteretic loop became wider and larger plastic deformation remained. In this case, the energy was dissipated by the forming of larger plastic deformation, suggesting that premature failure of the columns occurred at small displacement level. This is consistent with the previous observation that the ultimate displacement of the column decreased by about 15% when the loading direction increased from 0° to 60°,

ACCEPTED MANUSCRIPT

although the energy dissipation was approximately the same at the same displacement level.

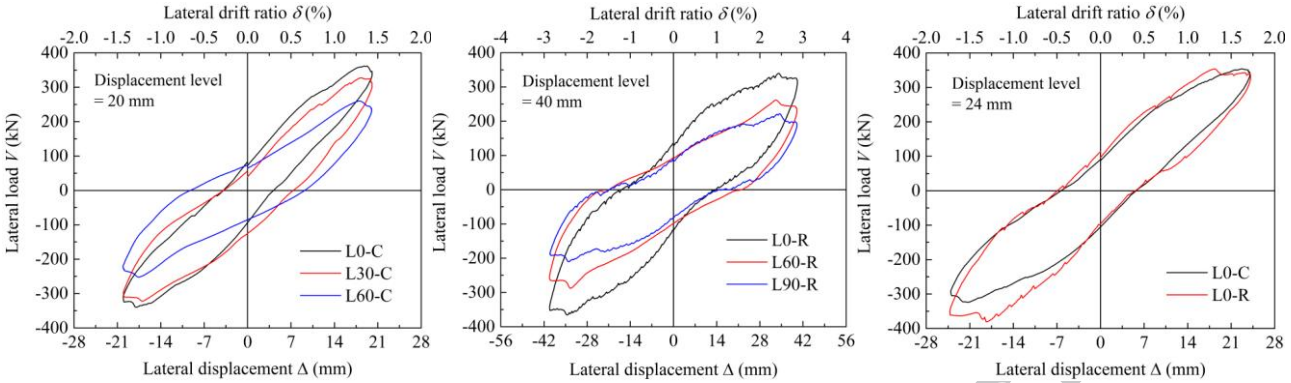

(a) Control (b) Retrofitted (c) L0-C and L0-R

Fig. 16 Comparison of single hysteretic loop at the same displacement level

For retrofitted specimens, the energy dissipation capacity was generally reduced with the increase of loading direction angle, as shown in Fig. 15 (b). This is due to the reduction in the lateral strength of retrofitted specimens with the increase of loading angle. The comparison of hysteretic loops of retrofitted specimens that were loaded in different directions is shown in Fig. 16 (b). It is evident that the lateral strength decreased with the increase of loading direction angle, but the width of the hysteretic loops was approximately the same and the plastic deformation was only slightly increased.

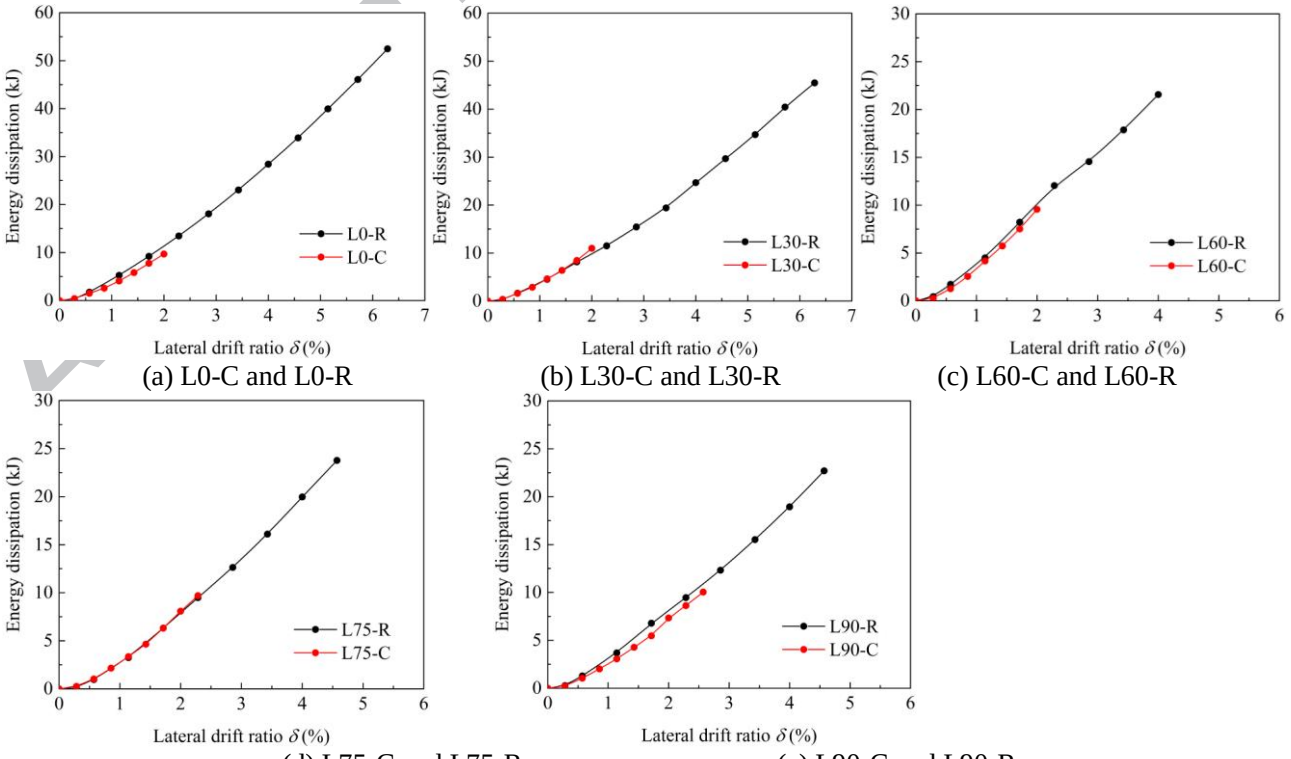

(a) L0-C and L0-R (b) L30-C and L30-R (c) L60-C and L60-R

(d) L75-C and L75-R (e) L90-C and L90-R

Fig. 17 Comparison of energy dissipation between control and retrofitted columns

Fig. 17 shows the single loop energy dissipation versus lateral drift ratio for control and retrofitted specimens in each loading direction. It was found that the retrofitted columns generally had larger hysteretic energy dissipation capacity than the control specimens at the same displacement levels in most loading directions. The comparison of single hysteretic loop between control and corresponding retrofitted specimens at the same displacement level also confirmed that the hysteretic loop of retrofitted specimen enclosed slightly larger area than that of corresponding control specimen, as shown in Fig. 16 (c).

4. Conclusions

An experimental study was carried out on five un-retrofitted and five FRP-retrofitted rectangular RC columns under combined constant axial compression and reverse lateral loading in different directions. Based on interpretations and discussions of the test results, the following conclusions can be drawn:

(1) The loading direction had significant effects on the seismic performance of both un-retrofitted and retrofitted rectangular RC columns. The lateral drift, shear resistance and energy dissipation capacities generally decreased with the increase of lateral loading direction angle. The failure of un-retrofitted control columns generally varied from brittle shear failure mode to ductile flexural failure mode when the lateral load direction varied from the strong axis direction (i.e. 0°) to the weak axis direction (i.e. 90°). All the retrofitted specimens exhibited ductile failure mode despite the variation of lateral loading directions.

(2) The seismic performance of rectangular RC columns was obviously improved after being retrofitted with CFRP, despite the variation in the loading direction. However, the efficiency of the CFRP retrofitted strategy decreased with the increase of lateral loading direction angle.

(3) The shear strength of both un-retrofitted and FRP-retrofitted rectangular RC columns generally agreed with the ellipse-interaction line. The lateral strength of both un-retrofitted and retrofitted rectangular RC columns in nonprincipal directions can be reasonably predicted based on the

ACCEPTED MANUSCRIPT

lateral strength in the principal directions by the ellipse relationship.

(4) Both un-retrofitted and CFRP-retrofitted rectangular RC columns generally exhibited worst ultimate lateral deformation and plastic deformation capacities when the lateral loading was in the 60° direction; the performance was even much worse than that in the weak axis direction (i.e. 90°). The 60° direction was shown to be another weak axis or even the critical weakest axis for both un-retrofitted and retrofitted rectangular RC columns.

Acknowledgments

This research was supported by the National Natural Science Foundation of China (Grant No. 51408153, No. 51478143, and No. 51278150) and the China Postdoctoral Science Foundation (Grant No. 2014M551252 and No. 2015T80354).

References

[1] Rodrigues H, Varum H, Arêde A, Costa A. Behaviour of reinforced concrete column under biaxial cyclic loading-state of the art. Int J Adv Struct Eng 2013; 5(1):4.

[2] Saatcioglu A, Ozcebe G. Response of reinforced concrete columns to simulated seismic loading. ACI Struct J 1989; 86(1):3-12.

[3] Lehman D, Moehle J, Mahin S, Galderone A, Henry L. Experimental evaluation of the seismic performance of reinforced concrete bridge columns. J Struct Eng 2004; 130(6):869-879.

[4] Hindi R, Turechek W. Experimental behavior of circular concrete columns under reversed cyclic loading. Constr Build Mater 2008; 22:684-693.

[5] Xiao JZ, Zhang C. Seismic behavior of RC columns with circular, square and diamond sections. Constr Build Mater 2008; 22:801-810.

[6] Barbosa AR, Link T, Trejo D. Seismic performance of high-strength steel RC bridge columns. J Bridge Eng 2016; 21(2): 04015044.

ACCEPTED MANUSCRIPT

[7] Burgueno R, Babazadeh A, Fedak LK, Silva PF. Second-order effects on seismic response of slender bridge columns. ACI Struct J 2016; 113(4):735-746.

[8] Seible F, Priestley MN, Hegemier GA, Innamorato D. Seismic retrofit of RC columns with continuous carbon fiber jackets. J Compos Constr 1997; 1(2):52-62.

[9] Xiao Y, Ma R. Seismic retrofit of RC circular columns using prefabricated composite jacketing, J Struct Eng 1997; 123(10):1357-1364.

[10] Wu YF, Liu T, Wang L. Experimental investigation on seismic retrofitting of square RC columns by carbon FRP sheet confinement combined with transverse short glass FRP bars in bored holes. J Compos Constr 2008; 12(1):53-60.

[11] Gu DS, Wu ZS, Wu YF. Confinement effectiveness of FRP in retrofitting circular concrete columns under simulated seismic load. J Compos Constr 2010; 14(5):531-540.

[12] Dai JG, Lam L, Ueda T. Seismic retrofit of square RC columns with polyethylene terephthalate (PET) fiber reinforced polymer composites, Constr Build Mater 2012; 27(1):206-217.

[13] Liu J, Sheikh SA. Fiber-reinforced polymer-confined circular columns under simulated seismic loads. ACI Struct J 2013; 110(6):941-951.

[14] Ma G, Li H. Experimental study of the seismic behavior of predamaged reinforced-concrete columns retrofitted with basalt fiber-reinforced polymer. J Compos Constr 2015; 19(6): 04015016.

[15] Cai ZK, Wang DY, Smith ST, Wang ZY. Experimental investigation on the seismic performance of GFRP-wrapped thin-walled steel tube confined RC columns. Eng Struct 2016; 110:269-280.

[16] Wang DY, Wang ZY, Smith ST, Tao Y. Seismic performance of CFRP-confined circular

ACCEPTED MANUSCRIPT

high-strength concrete columns with high axial compression ratio. Constr Build Mater 2017; 134:91-103.

[17] Hadi MNS. Behaviour of FRP strengthened concrete columns under eccentric compression loading. Compos Struct 2007; 77:92-96.

[18] Pantelides CP, Gergely J, Reaveley LD. In-situ verification of rehabilitation and repair of reinforced concrete bridge bents under simulated seismic loads. Earthq Spectra 2001, 17(3):507-530.

[19] Pantelides CP, Duffin JB, Reaveley LD. Seismic strengthening of reinforced-concrete multicolumn bridge piers. Earthq Spectra 2007, 23(3):635-664.

[20] Bousias SN, Verzeletti G, Fardis MN, Gutierrez E. Load-path effects in column biaxial bending with axial force. J Eng Mech 1995; 121(5):596-605.

[21] Lupoi G, Calvi GM, Lupoi A, Pinto PE. Comparison of different approaches for seismic assessment of existing buildings. J Earthq Eng Jan 2004; 08(spec01):121-160.

[22] Pham PT, Li B. Seismic behavior of reinforced concrete columns with light transverse reinforcement under different lateral loading directions. ACI Struct J 2013; 110(5):1-11.

[23] Rodrigues H, Arêde A, Varum H, Costa A. Experimental evaluation of rectangular reinforced concrete column behaviour under biaxial cyclic loading. Earthq Eng Struct Dyn 2013; 42(2):239-235.

[24] Rodrigues H, Furtado A, Arêde A. Behavior of rectangular reinforced-concrete columns under biaxial cyclic loading and variable axial loads. J Struct Eng 2016; 142(1):04015085.

[25] Shirmohammadi F, Esmaeily A. Performance of reinforced concrete columns under bi-axial lateral force/displacement and axial load. Eng Struct 2015; 99:63-77.

[26] Campione G, Cavaleri L, Di Trapani F, Macaluso G, Scaduto G. Biaxial deformation and

ACCEPTED MANUSCRIPT

ductility domains for engineered rectangular RC cross-sections: A parametric study highlighting the positive roles of axial load, geometry and materials. Eng Struct 2016; 107:116-134.

[27] Dong ZH, Han Q, Du XL, Zhang DJ. Experimental study on seismic performance of CFRP confined RC rectangular hollow section bridge piers. In: International Efforts in Lifeline Earthquake Engineering, Proceedings of the 6th China-Japan-US Trilateral Symposium on Lifeline Earthquake Engineering, May 2014. p.457-464.

[28] Rodrigues H, Arêde A, Furtado A, Rocha P. Seismic rehabilitation of RC columns under biaxial loading: An experimental characterization. Stuct 2015; 3:43-56.

[29] GBJ11-89. Code for seismic design of buildings. Ministry of Construction of the People's Republic of China, Beijing, China; 1989 (in Chinese).

[30] ASTM E8/E8M. Standard test methods for tension testing of metallic materials. American Society for Test and Materials (ASTM), West Conshohocken, PA, USA; 2008.

[31] Sheikh SA, Khoury SS. Confined concrete columns with stubs. ACI Struct J 1993; 90(4):414-431.

[32] Tirasit P, Kawashima K. Seismic performance of square reinforced concrete columns under combined cyclic flexural and torsional loadings. J Earthq Eng 2007; 11:425-452.

[33] Jiang C, Wu YF, Wu G. Plastic hinge length of FRP-confined square RC columns. J Compos Constr 2014; 18(4):04014003.

[34] Youssf O, ElGawady MA, Mills JE. Displacement and plastic hinge length of FRP-confined circular reinforced concrete columns. Eng Struct 2015; 101:465-476.

[35] ASTM D3039/D3009M-08. Standard test methods for tension properties of polymer matrix composite materials. American Society for Test and Materials (ASTM), West Conshohocken,

ACCEPTED MANUSCRIPT

PA, USA; 2008.

[36] GB50011-2010. Code for seismic design of buildings. Ministry of Housing and Urban-Rural Construction of China, Beijing, China; 2010 (in Chinese).

[37] Mahin S A, Bertero VV. Problems in establishing and predicting ductility in aseismic design. Proceedings of International Symposium on Earthquake Structural Engineering, St. Luis, Missouri, 1976. p.613-628.

[38] Mahin S A, Bertero VV. An evaluation of inelastic seismic design spectra. J Struct Div 1981; 107(ST9):1777-1795.

[39] GB50010-2010. Code for design of concrete structures. Ministry of Housing and Urban-Rural Construction of China, Beijing, China; 2010 (in Chinese).

[40] Clough RW, Penzien J. Dynamics of structures. McGraw Hill Inc., New York, 1993.